Dynamic Micro-Strain Analysis of Ultrafine-Grained Aluminum Magnesium Alloy Using Digital Image Correlation

YUZHENG ZHANG, TROY D. TOPPING, ENRIQUE J. LAVERNIA, and STEVEN R. NUTT

Tensile tests were performed *in situ* on an ultrafine-grained (UFG) Al-Mg alloy using a micro-tensile module in a scanning electron microscope. The micro-strain evolution was tracked and measured using digital image correlation (DIC). A fine random speckle pattern was required to achieve high resolution and accuracy of strain measurement using DIC. To produce the speckle pattern, a patterning method was developed using electron beam lithography to deposit a gold speckle pattern. The nanoscale feature size of this gold pattern (45 nm) was useful for identifying the micro-strain among individual grains of the UFG Al-Mg alloy. Microstructural aspects of the UFG Al-Mg alloy were revealed by analysis of electron backscattered diffraction (EBSD) patterns. Finally, the effect of the UFG Al-Mg alloy microstructure on the nanoscale deformation mechanism was investigated by combining EBSD and DIC data in a contour map. This combined technique provides a method for direct measurement of micro-strain and is potentially useful for deformation studies of a wide range of nanostructured materials.

DOI: 10.1007/s11661-013-1805-9

I. INTRODUCTION

UNDERSTANDING deformation and fracture mechanisms is essential to improving mechanical properties of new materials. Microscopic investigations of new materials commonly rely on transmission electron microscopy (TEM), scanning electron microscopy (SEM), and focused ion beam (FIB). In recent years, new characterization techniques and methods have evolved to exploit the capabilities of these instruments. For example, *in situ* SEM observation of micro-strain evolution has become an attractive approach for studying the deformation mechanisms of advanced structural materials. Likewise, the use of digital image correlation (DIC) has been extended to small-scale deformation measurements. In this work, we focus on the direct observation of how micro-strain evolves among the grains of an ultrafine-grained (UFG) Al-Mg alloy. To our best knowledge, no study has been done on the *in situ* micro-strain measurement of an UFG Al-Mg alloy using DIC at the sub-micron level.

DIC[1,2] is a non-contact, adaptable metrology technique for in-plane or out-of-plane strain field measurement that can be utilized on a variety of length scales ranging from civil engineering structures[3] to microstructures of metallic specimens.[4,5] The DIC algorithm tracks a grayscale pattern on the deforming surface step by step in a small area called a subset. To track the full-field surface deformation, an isotropic random speckle pattern is required on the specimen surface. This speckle pattern can be either intrinsic (from existing surface features) or extrinsic, as in a deposited pattern. The optimal feature size of a speckle pattern is reportedly 2 to 3 pixels for a recorded image.[6] Therefore, different patterning methods are needed to meet this requirement at different scales. While there have been multiple investigations reporting the use of DIC in making microscale strain measurements, one of the major challenges in such endeavors is producing a nanoscale, random, and isotropic speckle pattern required for DIC. In this study, the area of interest is only about 20 by 20 μm which requires a nanoscale speckle patterns for DIC analysis.

Various approaches have been employed to generate extrinsic DIC patterns on different substrates at reduced scales. The most common patterning method for small-scale DIC involves using a high quality airbrush to spray microscale paint patterns on a substrate.[7,8] Another convenient approach is generating grid patterns using a grid mask.[9,10] Intrinsic patterns are also available when the surface of specimens exhibited small-scale features.[11] Nanoparticles are often utilized for DIC patterns because of the small sizes and low cost.[12,13] In addition, FIB systems have been used to deposit platinum dots in a slow and controllable process.[13] However, all of these studies highlight certain common drawbacks of the patterning methods employed, including lack of pattern density control, coarse feature size, non-random patterns, and substrate dependence.

In this work, e-beam lithography (EBL) was used to make nanoscale gold speckle patterns on the aluminum surface. EBL was introduced by Sutton *et al.*[19] as a DIC

YUZHENG ZHANG, Ph.D. Candidate, and STEVEN R. NUTT, Professor, are with the Department of Chemical Engineering and Materials Science, University of Southern California, Los Angeles, CA 90089-0241. Contact e-mail: yuzhengz@usc.edu TROY D. TOPPING, Post Doctorate, and ENRIQUE J. LAVERNIA, Professor, are with the Department of Chemical Engineering and Materials Science, University of California, Davis, CA 95616.

Manuscript submitted March 18, 2013.
Article published online May 23, 2013

patterning method. However, patterns from the early works were not small enough for a DIC analysis among the ultrafine grains. In this study, EBL parameters were optimized to achieve a 45-nm gold dot pattern in an area of 20 by 20 μm. EBL is commonly used for IC (integrated circuit) fabrication in the semiconductor industry and to produce nanoscale functional devices. EBL utilizes a focused electron beam to generate patterns across a resist-coated substrate. A polymer resist film is required as an electron beam resist layer. One conventional positive resist material for EBL is polymethyl-methacrylate (PMMA). As the highly focused electron beam scans across the resist following the pattern design, the areas exposed by the beam can be subsequently dissolved in a developer solution, while the remaining unexposed PMMA remains intact in the developing process. Subsequently, the pattern on the resist layer can be transferred to the substrate *via* post-developing processes such as direct etching and lift-off according to different applications. Finally, the residual polymer resist material can be simply dissolved away with acetone. The EBL patterning method is substrate independent, repeatable, and designable. The feature size limit of EBL patterns is determined primarily by the proximity effect attributed to electron forward- and backscattering in the resist layer.[14]

After the specimen was patterned, tensile tests were performed *in situ* in a SEM using a micro-tensile testing module. To reveal the effect of microstructure on deformation evolution, DIC strain analysis was performed on deformed samples and later correlated with a crystalline orientation map obtained using the electron backscattered diffraction (EBSD) technique.

II. EXPERIMENTS

A. *Specimen Preparation*

The bulk specimens used in this investigation were consolidated from cryomilled AA 5083 (Al-4.4Mg-0.7Mn-0.15Cr wt pct) powders produced by Valimet, Inc. (Stockton, CA). Cryomilling was performed in liquid nitrogen for 8 h using a modified Szegvari attritor. Stainless steel milling balls were used with a 32:1 ball-to-powder weight ratio. During the milling, 0.2 wt pct "stearic acid" (stearic acid:palmitic acid = 1:1) was added as a process control agent (PCA). Because of the large scale of the project, cryomilling was performed by a commercial entity (DWA Aluminum Composites, operating under the supervision of UC Davis and Pratt and Whitney Rocketdyne, Inc., Canoga Park, CA). After milling, the powder was transferred to a glove box in a liquid nitrogen medium, insuring that atmospheric contamination of the cryomilled powders was minimized. Further details of cryomilling are available elsewhere.[15–17]

After cryomilling, the powders were canned and hot vacuum degassed to remove the PCA and physi-adsorbed moisture prior to consolidation by quasi-isostatic (QI) forging (Advanced Materials and Manufacturing Technologies, LLC, AM2T, Granite Bay, CA). QI forging was conducted in two steps at 623 K (350 °C), followed by hot rolling at 450 °C in multiple steps (Niagara Specialty Metals, Akron, NY). After rolling, the UFG plate dimensions were ~19 mm in thickness and ~610 mm in diameter. Details pertaining to the processing and subsequent properties of this plate have been reported elsewhere.[18]

Miniature dog bone tensile specimens were produced by electrical discharge machining (EDM) and featured gage (aligned with the rolling direction) dimensions of 4 mm (length) × 3 mm (width) × 1.5 mm (thickness) as shown in Figure 1. A notch 200 μm wide and 500 μm long was machined in the center of the gage section to introduce stress concentration. As load was applied, plastic deformation was initially confined to the near-notch area, constraining the strain-localized area for DIC analysis.

As a reference point to conventional tensile data, a cylindrical ASTM E8M subsize specimen[5] was tested in addition to the miniature dog bone specimen used for DIC analysis. The subsize specimen had nominal dimensions of ~15 mm gage length × ~3 mm diameter.

B. *Alignment of EBSD Scanned Area to DIC Strain Field*

Grain structures were revealed using EBSD. During an EBSD scan, the diffraction pattern generated was indexed by matching to a library of Kikuchi patterns. An EBSD scan was conducted prior to EBL speckle patterning because the residual polymer layer would block the scattered signal from the sample beneath it. Before scanning, the tensile specimen was ground and polished through 240, 400, 600, 1200, 2400, and 4000 grit abrasive papers and diamond suspensions (6, 3, and 1 μm). Finally, the specimen was fine polished using colloidal silica suspension on a vibratory polisher (Buehler) for 1 hour until the surface showed a mirror-like finish. To later match the region of interest (ROI) with the EBSD scan region, reference marks were first deposited using EBL patterning, as shown in Figure 2(b). Direct observation of the ROI was not possible in the EBL machine because electrons' exposure from

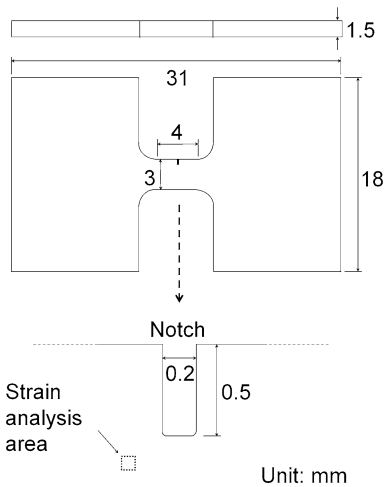

Fig. 1—Geometry of a dog bone tensile specimen and the notch area.

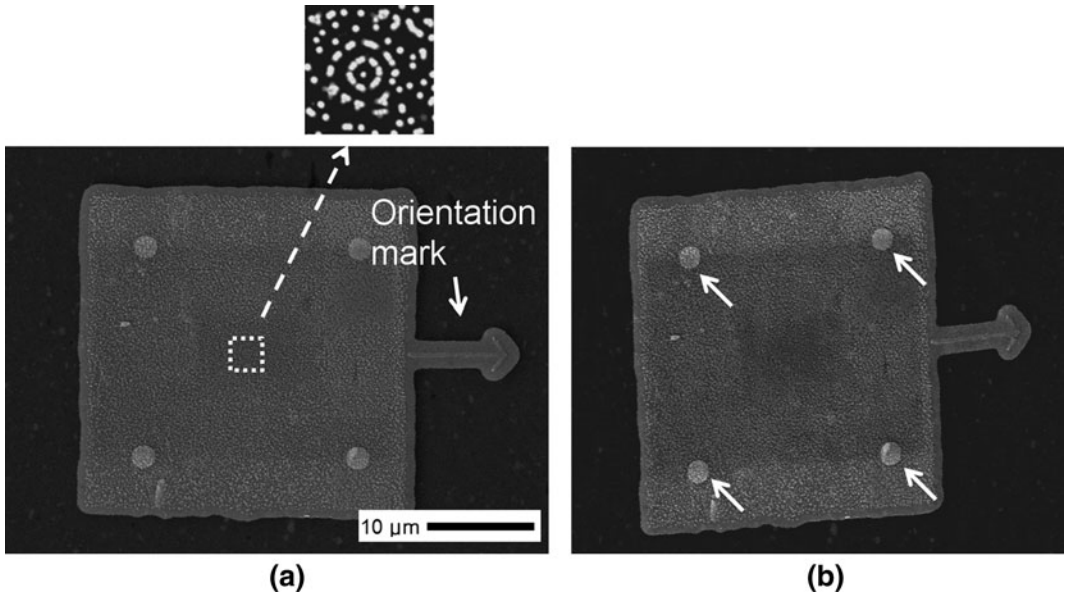

Fig. 2—(*a*) A random speckle pattern with a central target mark; (*b*) the same pattern after deformation; the arrows indicate the positions of reference marks.

imaging would cause unfavored patterns on the ROI. A Cartesian coordinate on the sample surface was therefore necessary to locate the ROI in EBL. Three additional reference marks were required for this coordinate on the sample surface. These three marks were situated far from the ROI to allow locating the area without exposing it to electrons.

An EBSD scan of the ROI was carried out at 15 kV acceleration voltage, with a probe current of 13 and a working distance of 15 mm using JEOL JSM-7001F SEM with an EDAX TSL orientation image mapping system. An area of 20 × 20 μm was mapped using a step size of 50 nm. The raw EBSD data was first processed using a grain confidence index (CI) standardization procedure. A secondary process called single iteration grain dilation was carried out to reduce unindexed points and noise level. Following the EBSD scanning, the speckle pattern was transferred onto the scanned area using EBL. Using these reference marks, we were able to insure that the EBSD scanned area matched the EBL patterned area for DIC analysis.

C. *E-Beam Lithography (EBL) Patterning*

The polished surface was first spin coated with PMMA A4 at 5000 rpm for 30 seconds. Post-baking of the coated sample was carried out on a hot plate at 453 K (180 °C) for 2 minutes. To achieve a fine EBL pattern, the smallest aperture (7.5 μm) and a low acceleration voltage (10 kV) were selected. A dosage test was performed to determine the optimal dose factor. The pattern designed by the CAD software consists of a 30 by 30 μm speckle pattern and an orientation mark as shown in Figure 2(a). After this pattern was transferred onto the PMMA layer, the sample was immediately developed by immersing in IPA:MIBK (3:1) solution for 45 seconds. The exposed PMMA regions were dissolved away during the developing process. After developing, the sample was rinsed in IPA for 1 minute and dried using compressed air. To harden the residual polymer layer, the sample was again baked at 373 K (100 °C) for 2 minutes. A layer of gold 20 nm thick was then deposited using a sputter coater. Finally, the residual PMMA was dissolved using acetone.

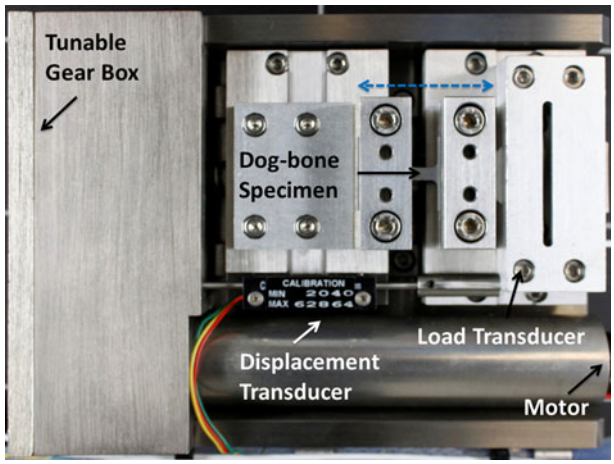

Fig. 3—Micro-tensile stage placed in SEM chamber.

D. *In Situ Micro-Tensile Testing*

Micro-tensile tests were carried out *in situ* in a SEM vacuum chamber at room temperature using the micro-tensile module shown in Figure 3. The dimensions of the micro-tensile stage (146 mm × 108 mm × 39 mm) are small enough to be placed inside a SEM chamber. Mounted inside a SEM vacuum chamber, the micro-tensile stage can be controlled by a computer and a control unit *via* a feed-through. The micro-tensile

module was capable of achieving a maximum load of 5 kN. The SEM used in this study (JEOL JSM-6610) featured a tungsten filament, and image distortion was evaluated prior to the actual tensile test. A series of SEM images were recorded prior to deformation of the sample. DIC analysis was then conducted on these non-deformed images to determine the pseudo-strain introduced by image distortion. This distortion effect was minimized to 0.01 pct by reducing the specimen charging effect and by image averaging. Details of distortion correction will be discussed later.

A strain rate of 4.18×10^{-4} s^{-1} was selected for a quasi-static tensile testing. During micro-tensile tests, SEM images were recorded after the test was interrupted every 5 seconds. After each stop, the sample was held for at least 1 minute to allow the load to stabilize. To insure that each image was captured in an identical position, a target mark was designed in the center of the speckle pattern as shown in Figure 2(a). Each deformed image was aligned by centering on the target at a higher magnification. Secondary electron images were acquired, and the acceleration voltage and the working distance were set to 15 kV and 12 mm, respectively, to minimize the charging effect.

E. *In-Plane Micro-Strain Analysis*

A series of deforming images were imported into the 2D-DIC software (VIC-2D, Correlated Solutions Inc.), and an undeformed image was used as a reference image. Deformed images were then compared to the first reference image. All the SEM images were recorded at the same magnification with a spatial resolution of 13.7 nm $pixel^{-1}$. During deformation, the grayscale speckle pattern was tracked in a small window termed the subset. A subset size of 70 and step size of 1 were selected. The correlation process was initiated from the central target area. Finally, Lagrangian strains were calculated based on the relative displacement of speckle patterns.

III. RESULTS AND DISCUSSION

A. *EBL Random Speckle Pattern for DIC*

A gold speckle pattern was deposited on the sample surface using EBL, and dosage tests were performed to determine the optimal dose level. The base dose level was 800 pAs cm^{-2}. The total dose level was the base level multiplied by a dose factor. Figure 4 shows patterns produced with dose factors of 1, 2, 5, and 7. Dose factors of 1 and 2 both generated patterns with horizontal gold rods because the dose level was not sufficient to make holes through to the aluminum substrate. On the other hand, dose factors of 5 and 7 resulted in vertical gold columns—ideal for the DIC speckle pattern. To minimize the exposure time, a dose factor of 5 was selected. These gold columns had an

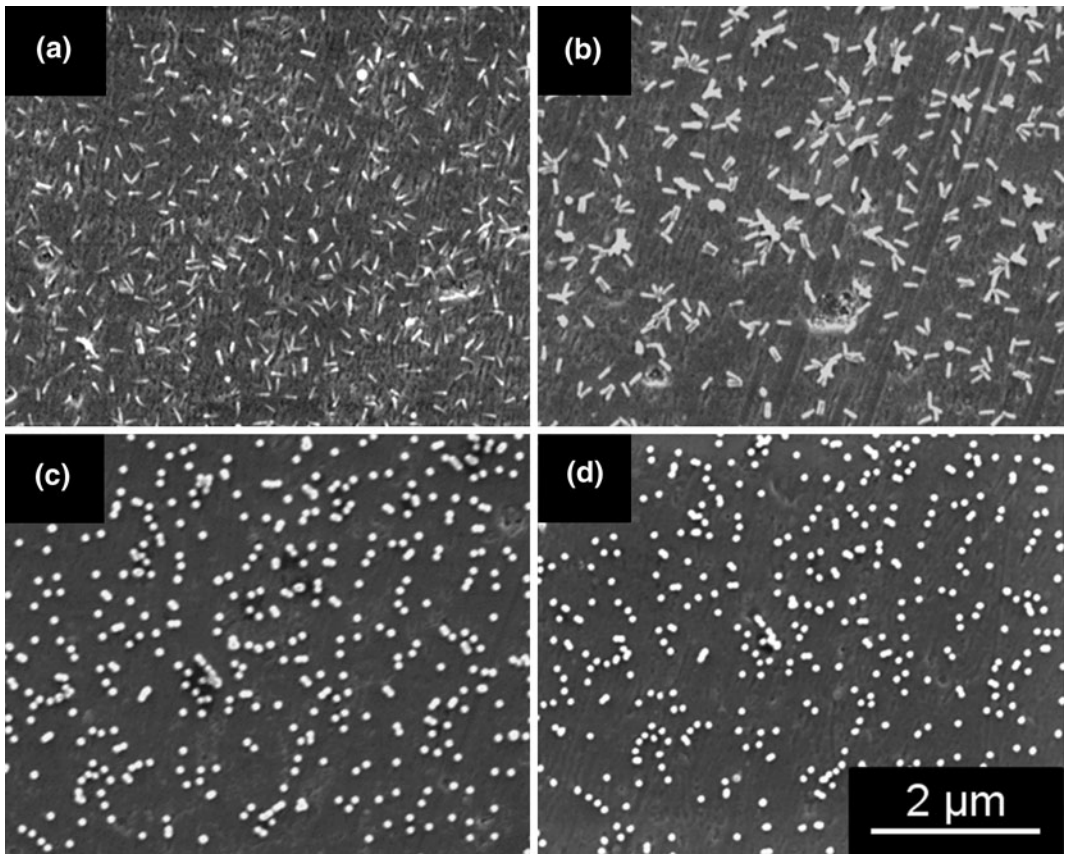

Fig. 4—EBL patterns with exposure (*a*) dose factor 1, (*b*) dose factor 2, (*c*) dose factor 5, and (*d*) dose factor 7.

average height of 20 nm, insuring that good contrast could be achieved *via* secondary electron imaging (SEI). Because SEI does not rely on atomic number contrast, this DIC pattering method is generally substrate independent.

The diameter of the gold columns is ~45 nm, which is close to the optimal feature size (40 nm) for a 20 by 20 μm field of view.[6] To evaluate the pattern quality, a pattern intensity histogram was constructed, as shown in Figure 5. This grayscale (from 0 to 255) histogram is plotted against the numbers of pixels. As shown in Figure 5, a bell-shaped distribution of pattern intensity was observed. Patterns with a bell-shaped intensity distribution are ideal for accurate correlation results.[8] Because of the small feature size and high contrast, the EBL pattern is well suited to sub-micron DIC analysis for the UFG Al-Mg alloy.

B. *Intrinsic Image Distortion Correction*

The accuracy of the *in situ* DIC analysis depends on the quality of the speckle pattern and the SEM images. SEM imaging quality is limited by the SEM resolution, specimen contrast, and the intrinsic image distortion. Although SEM provides sufficient resolution and contrast for the current DIC analysis, image distortion can degrade the correlation accuracy, especially at higher magnifications. Pseudo-strain can be introduced due to image distortion (as opposed to real surface deformation).

To evaluate the influence of image distortion, a series of images of the same region before loading were recorded at different times. Pseudo-strain was calculated by correlating to the reference image taken at $t = 0$ second. A random distribution of pseudo-strain was observed at five different time delays. This pseudo-strain was not spatial but temporal distortion in nature. The average value of the pseudo-strain introduced by image distortion was plotted in Figure 6. The average value of the pseudo-strain was independent of the time lapse. The effect of image distortion can be minimized using an image integration process that averages image data from multiple scans.[19] In this study, the scan speed was set to 20 seconds per scan and the averaging number of 2 was selected. Therefore, two images were integrated together with a total scan time of 40 seconds. Compared to a single 40-second scan, the integrated image has a higher signal-to-noise ratio and a more homogeneous pseudo-strain distortion instead of step changes in x and y directions.[19] As shown in Figure 6, the average and the maximum value of this pseudo-strain for the SEM used (JEOL JSM-6610) is on the order of 0.01 and 0.5 pct, respectively.

C. *Micro-Strain Measurement of Ultrafine-Grained Al-Mg Alloy*

1. *Micro-tensile testing results*

Micro-tensile tests were performed at room temperature using a constant strain rate of 4.18×10^{-4} s^{-1}. The engineering stress–strain curve obtained from a micro-tensile stage is shown in Figure 7. The engineering stress was calculated using the applied load divided by the cross section of the gage length (1.5 × 3 mm). The engineering strain was defined by the change of the gage length divided by the original gage length (4 mm). The micro-serrations occurred when the test was interrupted for imaging. The sudden drop of stress followed by gradual increase at each serration was caused by dislocation relaxation processes.[20] The mechanical properties of the UFG Al-Mg alloy, including Young's modulus, 0.2 pct offset yield strength, ultimate tensile strength (UTS), and elongation, are tabulated in Table I. As a comparison, tensile data extracted from a standard tensile test (ASTM E8M) are also listed in Table I.

2. *In-plane micro-strain evolution among grains*

The patterned area was located along one of the shear bands near the notch where the shear strain was initially localized due to the stress concentration. Figure 2(b) shows the patterned area after plastic deformation.

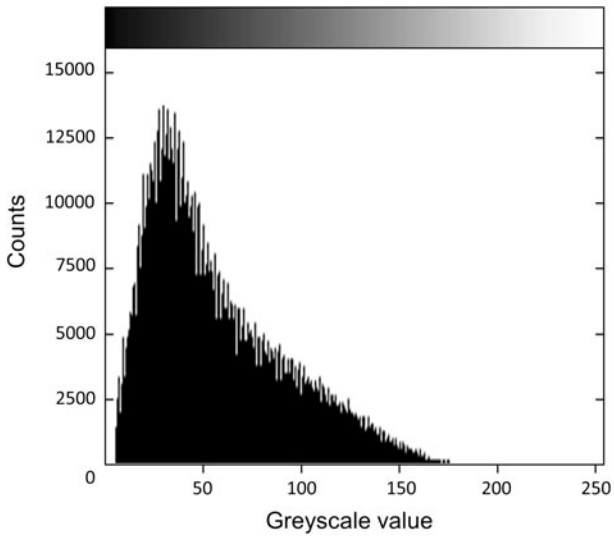

Fig. 5—Pixel grayscale histogram of the EBL speckle pattern.

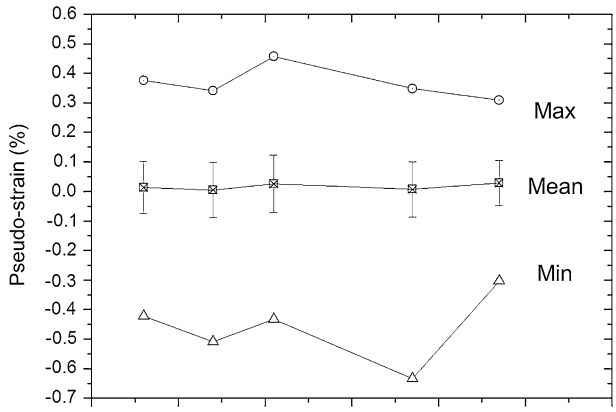

Fig. 6—Pseudo-strain introduced by SEM image distortion.

Because the patterned area was located along the shear band, the shear strain e_{xy} was the major strain component during deformation.

The EBSD inverse pole figure map of the UFG Al-Mg alloy is shown in Figure 8. An average CI of 0.65 was achieved, indicating that above 90 pct of the data points are indexed correctly. The UFG Al-Mg alloy has an average grain size of 560 nm with a fraction of 92.4 pct high-angle grain boundaries (15 deg to 180 deg misorientation) and 7.6 pct low-angle grain boundaries (5 deg to 15 deg misorientation). The black regions in Figure 8 are regions in which the CI was less than 0.1. Low values of CI can be caused by uneven surfaces, voids, highly deformed grains, or non-crystalline phase. The black areas at the four corners are caused by the reference marks which are covered with a layer of polymer. The large low-CI area in the top part of the map is due to the presence of voids. The rest of the low-CI regions are attributed to uneven areas or residual polishing debris deposited during the polishing process.

Finally, the EBSD inverse pole figure was overlaid on the correlated strain map by matching the four corner reference marks and the orientation mark. The micro-strain evolution (Figure 9) was recorded from 180 to 240 seconds of the micro-tensile test, during which the macro-strain increased from 9.3 to 12.1 pct.

As evident from Figure 9, the micro-strain did not initiate uniformly over the entire area. The strain was localized within larger grains and extended across grain boundaries into adjacent smaller grains. This observation is consistent with the bimodal deformation model proposed by Lee *et al.*[21] who claimed that larger grains were likely to exhibit larger plastic deformation than fine grains and also reported that micro-voids and cracks nucleated at interfaces of coarse and fine grains due to localized deformation. This phenomenon was first observed using a light microscope at a much lower magnification and resolution.[22] The EBL nanoscale patterning method in the present work affords the opportunity to observe the micro-strain evolution within individual grains of the UFG Al-Mg alloy. However, micro-voids and cracks were not observed because of the polymer layer covering the patterned area.

The average micro-strain is plotted as a function of time in Figure 10. The average value of the micro-strain saturated at about 220 seconds because a major crack developed and propagated along the shear band on the opposite side of the notch root.

Note that the combined EBSD and DIC metrology described here is valid only when the micro-strain is relatively low (less than 10 pct). Larger deformations can limit the use of EBSD for the reasons that (1) a distorted crystalline structure generates unrecognizable diffraction patterns and (2) large distortions of grain geometry hamper accurate matching between the DIC micro-strain field and the EBSD inverse pole figure map. Moreover, *in situ* EBSD is not always feasible due to space constraints within the SEM vacuum chamber and the long processing time for a single EBSD scan. Alternative methods will be required to reveal a deforming microstructure and perform *in situ* tensile testing simultaneously.

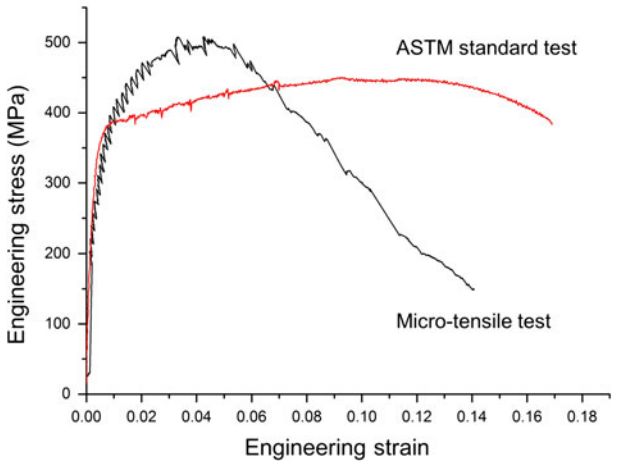

Fig. 7—Engineering stress and strain curve for the UFG Al-Mg alloy.

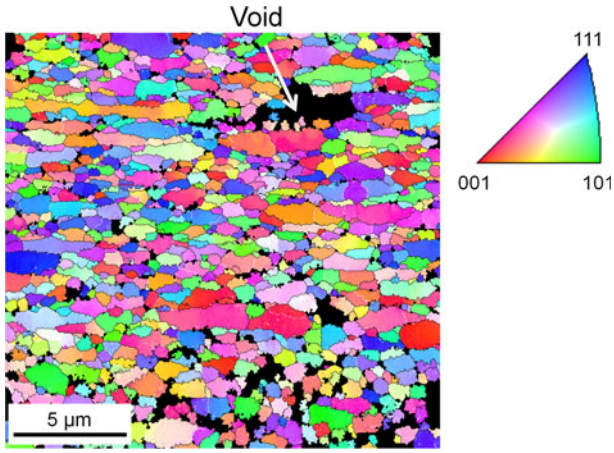

Fig. 8—EBSD inverse pole figure map for the UFG Al-Mg alloy; black and white boundaries indicate high-angle grain boundaries and low-angle grain boundaries, respectively.

Table I. Mechanical Properties of the UFG Al-Mg Alloy

	Young's Modulus (GPa)	Yield Strength σ_y (MPa)	UTS (MPa)	Elongation to Failure (pct)
UFG Al-Mg Alloy (Micro-tensile)	63	397	503	14.6
UFG Al-Mg Alloy (ASTM E8M)	70	370	450	16.9

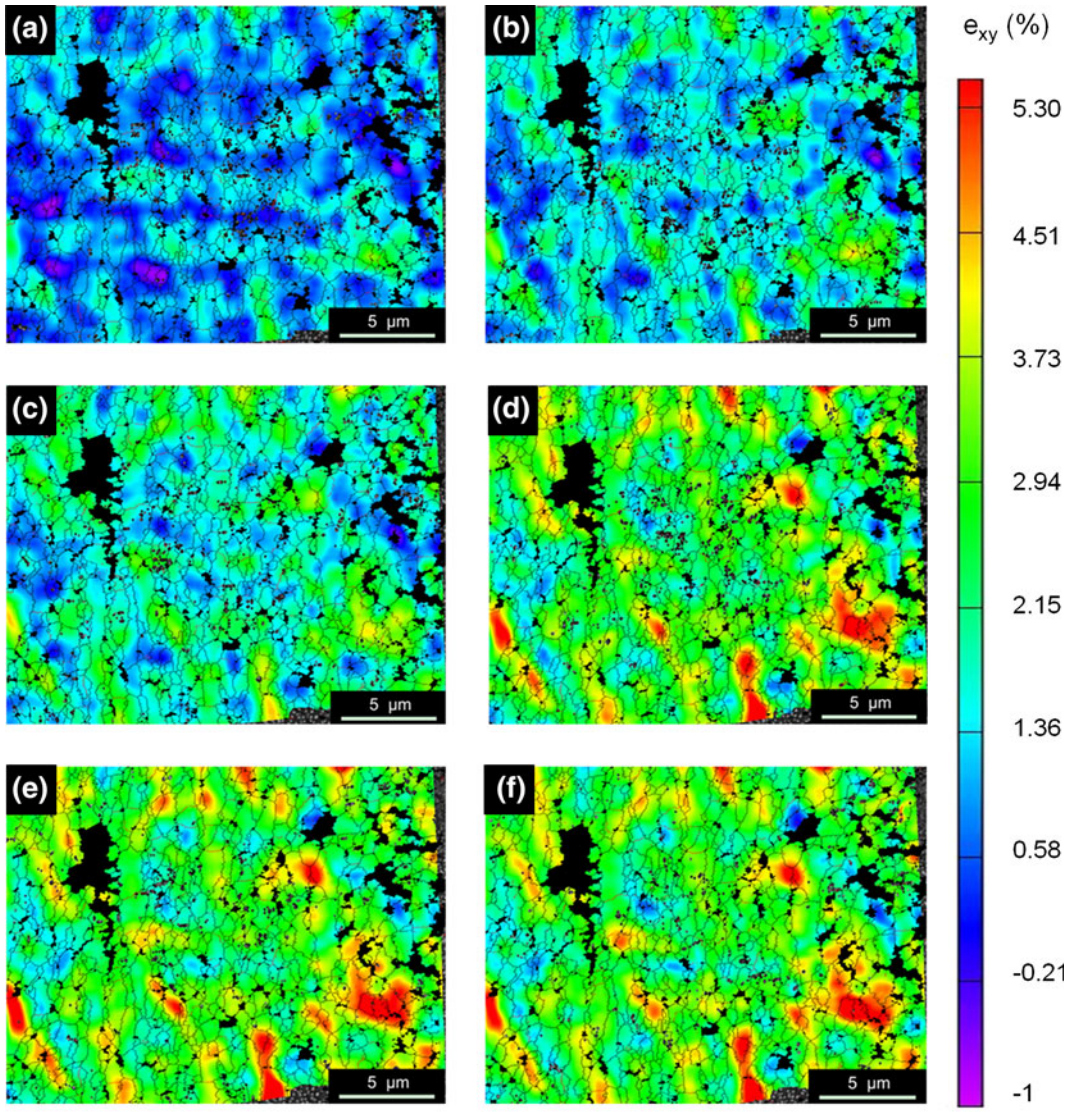

Fig. 9—Engineering shear strain e_{xy} overlapped with grain structures as a function of deformation time: (*a*) 180 s, (*b*) 190 s, (*c*) 200 s, (*d*) 215 s, (*e*) 225 s, and (*f*) 240 s.

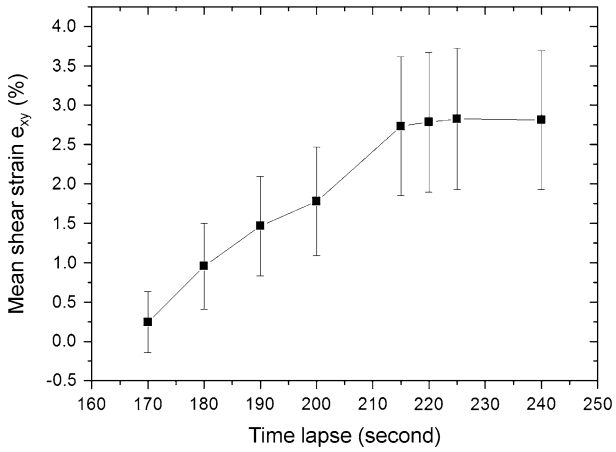

Fig. 10—The mean engineering shear strain evolution.

IV. CONCLUSIONS

In this work, the micro-strain evolution of an UFG Al-Mg alloy was measured for the first time at nano-scaled grain structures. The EBL patterning technique described here is essential to generate the requisite fine speckle patterns with a feature size of 45 nm. The EBL patterning method is repeatable, designable, scalable to various sizes, and substrate independent. Using the combined EBSD and DIC techniques, effects of micro-structural features can be investigated by overlaying the crystalline orientation map with the DIC strain contour map. Using these techniques, micro-strain localization was observed in large grains in an UFG Al-Mg alloy and extended across grain boundaries into adjacent smaller grains, indicating that larger grains were likely to exhibit larger plastic deformation than fine grains.

Micro-voids and cracks formed at interfaces of coarse and fine grains to maintain the discontinuity in strain field. The patterning method in this work is suitable for the direct observation of deformation mechanisms in a wide range of nanoscaled homogeneous and heterogeneous materials.

ACKNOWLEDGMENTS

The authors gratefully acknowledge B. Ahn, J. Ma, and Y. Zhao for their advice. The images and data used in this article were generated at The Center for Electron Microscopy and Microanalysis, the University of Southern California. Dr. T.D. Topping and Dr. E.J. Lavernia extend thanks and appreciation to the Materials Design Institute, funded by the LANL/UC Davis Education Research Collaboration, Los Alamos National Laboratory (LANS Subcontract No. 75782-001-09). Gratitude is also extended to Mr. Rodney Peterson and Dr. William Golumbfskie of the Office of Naval Research for support of this work (ONR Contract N00014-12-C-0241).

REFERENCES

1. W.H. Peters and W.F. Ranson: *Opt. Eng.*, 1982, vol. 21, pp. 427–32.
2. M.A. Sutton, W.J. Wolters, W.H. Peters, W.F. Ranson, and S.R. McNeill: *Image Vis. Comput.*, 1983, vol. 1 (3), pp. 1333–39.
3. S. Yoneyama, A. Kitagawa, S. Iwata, K. Tani, and H. Kikuta: *Exp. Tech.*, 2007, vol. 31, pp. 34–40.
4. M.A. Tschopp, B.B. Bartha, W.J. Porter, P.T. Murray, and S.B. Fairchild: *Metall. Mater. Trans. A*, 2009, vol. 40A, pp. 2363–68.
5. J. Kang, Y. Ososkov, J.D. Embury, and D.S. Wilkinson: *Scripta Mater.*, 2007, vol. 56, pp. 999–1002.
6. P. Zhou and K.E. Goodson: *Opt. Eng.*, 2001, vol. 40, pp. 1613–20.
7. N.K. Kar, Y. Hu, B. Ahn, and S.R. Nutt: *Compos. Sci. Technol.*, 2012, vol. 72 (11), pp. 1283–90.
8. T.A. Berfield, J.K. Patel, R.G. Shimmin, P.V. Braun, J. Lambros, and N.R. Sottos: *Exp. Mech.*, 2007, vol. 47, pp. 51–62.
9. H. Jin, W.Y. Lu, and J. Korellis: *J. Strain Anal.*, 2008, vol. 43, pp. 719–27.
10. Y. Tanaka, K. Naito, S. Kishimoto, and Y. Kagawa: *Nanotechnology*, 2011, vol. 22, p. 115704.
11. B. Ahn and S.R. Nutt: *Exp. Mech.*, 2010, vol. 50, pp. 117–23.
12. H. Wang, H. Xie, Y. Li, and J. Zhu: *Meas. Sci. Technol.*, 2012, vol. 23, p. 035402.
13. A.D. Kammers and S. Daly: *Meas. Sci. Technol.*, 2011, vol. 22, p. 125501.
14. C. Vieu, F. Carcenac, A. Pépin, Y. Chen, M. Mejias, A. Lebib, L. Manin-Ferlazzo, L. Couraud, and H. Launois: *Appl. Surf. Sci.*, 2000, vol. 164 (1–4), pp. 111–17.
15. A.P. Newbery, B. Ahn, T.D. Topping, P.S. Pao, S.R. Nutt, and E.J. Lavernia: *J. Mater. Process. Technol.*, 2008, vol. 203 (1–3), pp. 37–45.
16. T.D. Topping, B. Ahn, Y. Li, S.R. Nutt, and E.J. Lavernia: *Metall. Mater. Trans. A*, 2012, vol. 43A, pp. 505–19.
17. D.B. Witkin and E.J. Lavernia: *Prog. Mater. Sci.*, 2006, vol. 51 (1), pp. 1–60.
18. T.D. Topping, Y. Li, E.J. Lavernia, K. Manigandan, and T.S. Srivatsan: *Adv. Mater. Res.*, 2011, vol. 410, pp. 175–86.
19. M.A. Sutton, N. Li, D.C. Joy, A.P. Reynolds, and X. Li: *Exp. Mech.*, 2007, vol. 47, pp. 775–87.
20. A. Seeger: *Mater. Sci. Eng. A*, 2004, vol. 370, pp. 50–66.
21. Z. Lee, V. Radmilovic, B. Ahn, E.J. Lavernia, and S.R. Nutt: *Metall. Mater. Trans. A*, 2010, vol. 41A, pp. 795–801.
22. B. Ahn, E.J. Lavernia, and S.R. Nutt: *J. Mater. Sci.*, 2008, vol. 43, pp. 7403–08.